energies

MDPI

Article

Applying Deep Electrical-Resistivity Tomography Techniques for the Exploration of Medium- and Low-Geothermal Energy Resources

Cristina Sáez Blázquez *, Ignacio Martín Nieto, Javier Carrasco, Pedro Carrasco, Daniel Porras, Miguel Ángel Maté-González, Arturo Farfán Martín and Diego González-Aguilera

Department of Cartographic and Land Engineering, Higher Polytechnic School of Avila, University of Salamanca, Hornos Caleros 50, 05003 Avila, Spain; nachomartin@usal.es (I.M.N.); tgeofisicas@gmail.com (J.C.); retep81@usal.es (P.C.); dporras@geoland.es (D.P.); mategonzalez@usal.es (M.Á.M.-G.); afarfan@usal.es (A.F.M.); daguilera@usal.es (D.G.-A.)

* Correspondence: u107596@usal.es

Abstract: The growth of the geothermal industry demands the constant search of techniques with the aim of reducing exploration efforts whilst minimizing subsurface uncertainty. The exploration of geothermal resources is fundamental from the exploitation point of view, especially in those regions where this energy is not as widespread as the rest of renewable sources. This research shows how geoelectrical methods can contribute to the investigation and characterization of medium–low enthalpy geothermal resources until about 800 m of depth. A 2000 m long electrical-resistivity tomography profile was performed in a region of Southern Spain with previous evidence of moderate geothermal potential. Results of this geophysical campaign (together with a preliminary geological characterization) allowed for the obtainment of a 2D profile and a pseudo-3D model with extensive information about the subsoil in terms of geological composition and formations. The interpretation of geophysical results denotes the existence of a potential formation constituted by carbonate materials with thickness greater than 300 m, crossing different fractures. Once the ideal location for the geothermal exploitation is defined, the research evaluates the contribution of the possible energy source, deducing that the energy extraction in the potential fracturing area would be double that of the one in the vicinity of the site.

Keywords: geothermal resources; exploration; electrical resistivity tomography; 2D profile; potential area

Citation: Sáez Blázquez, C.; Martín Nieto, I.; Carrasco, J.; Carrasco, P.; Porras, D.; Maté-González, M.Á.; Farfán Martín, A.; González-Aguilera, D. Applying Deep Electrical-Resistivity Tomography Techniques for the Exploration of Medium- and Low-Geothermal Energy Resources. *Energies* **2024**, *17*, 1836. https://doi.org/10.3390/en17081836

Academic Editor: Hossein Hamidi

Received: 18 March 2024
Revised: 4 April 2024
Accepted: 9 April 2024
Published: 11 April 2024

1. Introduction

Due to the current energy context and the exponential increase of the world energy demand, there is a clear need to move towards the massive use of renewable energy resources and become less dependent on social or geopolitical factors. In fact, the continuous availability of energy is considered one of the most critical aspects for society development, especially considering that, today, a significant portion of energy still derives from burning limited organic fuels. One approach to replace conventional fossil fuels and alleviate the mentioned energy issues is the introduction of renewable energy technologies. In this sense, geothermal energy appears as a potential contributor in the way of reducing the external and internal energy dependence on non-renewable systems [1], constituting one of the most efficient sources that can operate continuously to meet the energy demand 24/7 [2]. This energy can be directly used for heating and/or cooling applications, constituting one of the oldest and most versatile ways of utilizing geothermal resources [3]. In this context, the globally installed capacity for direct geothermal use worldwide was, at the end of 2019, 107,727 MWt, meaning a 52% increase over the year 2015, which is a growing annual rate of 8.7% [4]. The reason for this significant growth is, mainly, the recent technological development of geothermal heat pumps (GHPs), which generally

constitute these shallow systems through the well-known ground-source or ground-water heat pump (GSHP-GWHP) technologies [5,6]. The alternative use of geothermal energy is power generation, which is usually attributed to deep and hydrothermal resources with an average growth rate of around 5% per year and a global production of 95 TWh in 2020 in more than 30 countries [7].

Despite the clear versatility of geothermal resources, when compared with other renewable solutions (e.g., biomass, hydro, solar PV, wind), geothermal falls far behind both in production and installed capacity. The principal obstacle to geothermal growth is the initial investment costs generally associated with power projects, but also for domestic heating and cooling solutions. However, numerous countries have done the required groundwork to conduct resource inventories with the aim of quantifying their potential for exploiting the different possibilities of geothermal energy [8,9].

In the particular case of Spain (where this research is focused), geothermal development is still undervalued. There are no high-enthalpy geothermal facilities operating in the country, and the shallow geothermal use is also limited. In this sense, although slower than desirable considering the existing capacity and energy requirements, the installation of GHP systems has been a growing trend in the last few years. In addition, public administrations are making a great effort to introduce GHP systems in public buildings (both in refitted and new spaces) in order to move into the concept of "Nearly Zero-Energy Buildings" (NZEBs) promoted by the European Union [10–13]. Based on the data from the World Geothermal Congresses of 2015 and 2020, the estimated uses for the country are summarized in the following Table 1.

Table 1. Estimated shallow geothermal uses for Spain [14,15].

Use	MWt	TJ/Year
Individual space heating	5.20	133.6
Greenhouse heating	22.0	165.4
Bath and swimming	3.80	92.0
Geothermal heat pumps	513.0	3542.0
Total for the country	**544.0**	**3933.0**

In spite of the clear advantages and the proven capacity to provide energy at a constant pace, as shown in the previous Table 1, the widespread production of geothermal energy in the country considered here has been limited by different factors. Among them are the lack of access to thermal supplies, the operating risks when drilling the geothermal wells, and the associated high capital costs [16,17]. When these factors are analyzed, it is common to conclude that most of these risks are mainly due to the lack of knowledge and precise characterization of the ground where the system is planned. In this sense, the in-depth evaluation of the subsoil structure and the determination of its expected thermal behavior are essential when designing the geothermal well field.

Regarding the reservoir temperature, it can be measured directly by bottom-hole temperature measurements. However, well measurements may not be representative of the entire reservoir, and geophysical prospecting appears as an effective tool for providing a more spatially complete information source. Depending on the type of geothermal system considered, the objective of these tests may be the determination of the geological structures and their distribution in depth, the estimation of the thermal properties of the existing formations, or the location of aquifers or singular structures, among many other applications [18–20]. The implementation of these techniques has proven to be useful when designing a shallow geothermal system and, thus, ensuring its correct operation during the estimated useful life period. But these prospecting systems are also essential when trying to achieve a better understanding of a deep geothermal resource. Geophysical detection and the monitoring of deep reservoirs represent a great advance in the exploration of geothermal

energy and, ultimately, in the acquisition of complete and optimized information about the structure in depth and the possibilities of future geothermal exploitation [21,22].

In the context of defining new possibilities of geothermal exploitation, this research includes a deep Electrical-Resistivity Tomography (ERT) model obtained from the geophysical prospecting on a certain study case, with an already known favorable geological setting and thermal evidence. From the geophysical campaign tests, the geological and thermal characterization of the area was performed to finally evaluate the possible geothermal use. Despite the preliminary discovery of anomalous underground temperatures, there is, in the study area, a lack of knowledge about the distribution of the geothermal resource at depth and the viability of its extraction. Based on this, the importance of this research lies in achieving a greater characterization of the underground area, being the final aim of the work is to provide a new basis for possible future geothermal exploitation. In turn, this research pursues to highlight the benefits of geophysics when characterizing the underground to evaluate the proper geothermal exploitation and optimize the configuration of the global well field and the corresponding elements of the system. In this context, the present paper is organized as follows: firstly, information about the geological and geothermal conditions of the study area and the geophysical technique implemented in the prospecting campaign is included. Then, the results of the geophysical tests are presented, as well as the discussion of the main achievements derived from the experimental phase. As a final section, the paper includes the conclusions and future perspectives of applications.

2. Preliminary Study-Area Characterization

2.1. Geology and Structural Setting

As previously mentioned, the objective of this study is the analysis of the subsoil characteristics in order to clarify the possibilities of future deep–medium geothermal energy exploitation. In this context, the study focuses on a certain area located in the autonomous community of Granada (Spain), in which an electrical-resistivity tomography survey has been performed. The following Figure 1 describes the location of the study area selected in the present research.

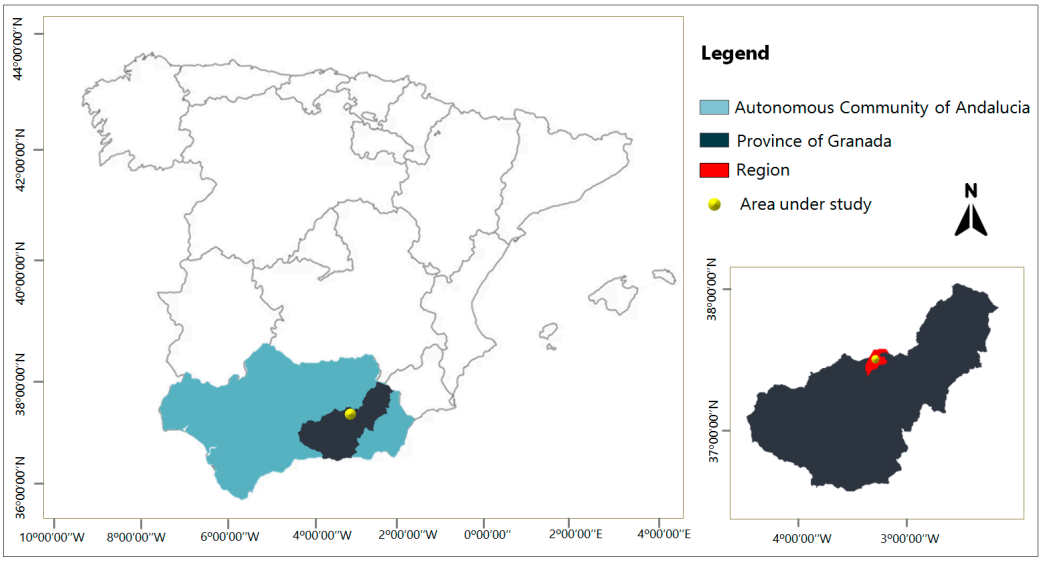

Figure 1. Location of the study area included in the evaluation of this research.

The selection of the location under study is based on the structural and geological characterization that indicated a possible formation of interest from the point of view of energy use. The area under study is located within a series of mountainous alignments to the south of the Guadalquivir Valley, known as the Baetic Mountains and, more specifically, in the region of the "Montes Orientales". The area suffered tectonic phenomena on a

continental scale during most of the Mesozoic and Tertiary, related to the opening of the Atlantic and Tethys, as well as the collision of the European and African plates [23,24]. In particular, the area included in this research is located in the sub-Baetic zone, characterized by presenting practically continuous sedimentation between the Triassic and the lower Miocene. Three main domains are established from north to south in this context:

- External sub-Baetic, corresponding to an area in which limestone materials predominate, acquiring great development levels of condensation.
- Medium sub-Baetic, predominating marly materials that appear as characteristic lithologies, radiolarites, and submarine volcanic rocks.
- Internal sub-Baetic that covers a relatively slightly subsiding sector in which exclusively limestone materials outcrop.

Beyond the described sub-Baetic level, Neogene and Quaternary materials are also located in the analysed environs that appear as alluvial deposits. Figure 2 presents the geological levels that constitute the area under study [25].

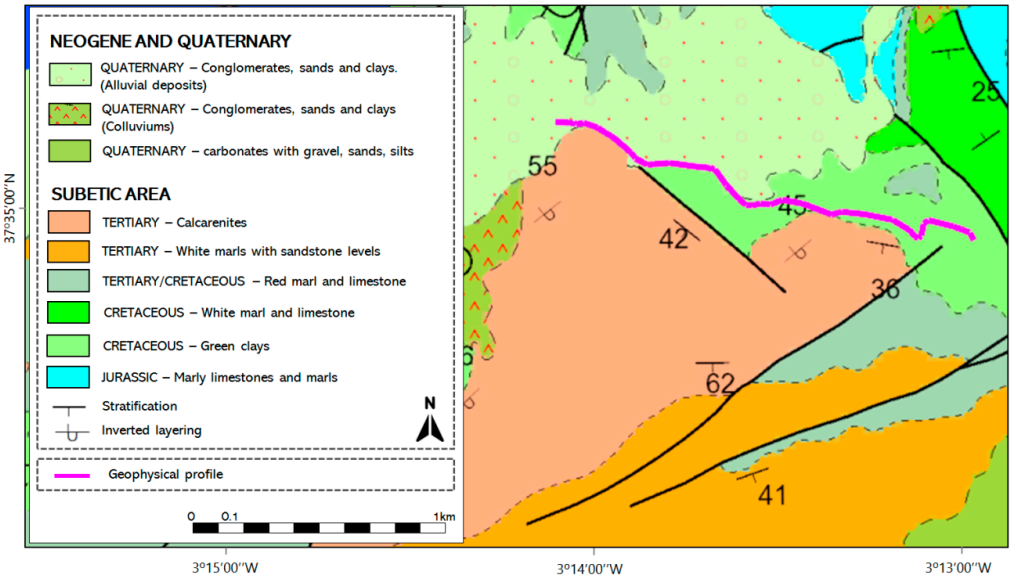

Figure 2. Geological setting of the area in which the geophysical survey was performed.

2.2. Previous Geothermal Evidences

In addition to the geological characterization presented above, in the vicinity of the area where the geophysical campaign has been conducted, there is an existing drilling whose open-access information is also relevant to the aim of this study. The 219 m borehole (included in Figure 3) was drilled by percussion with a downhole trephine and allowed for the deduction of the lithological column described in Table 2 [26].

During the prolonged pumping in the drilling, several measurements of the temperature of the extracted water were conducted. It was stabilized at 35.2 °C, which could preliminarily indicate the existence of a low-temperature geothermal resource (placing this temperature above the average of the place by around 15 °C). The interpretation of the borehole tests and the results of the pumping test also allowed for the conclusion that the storage formation has a calculated transmissivity of 600 m^2/day and an estimated exploitation flow of at least 60 L/s, with maximum values around 80–90 L/s.

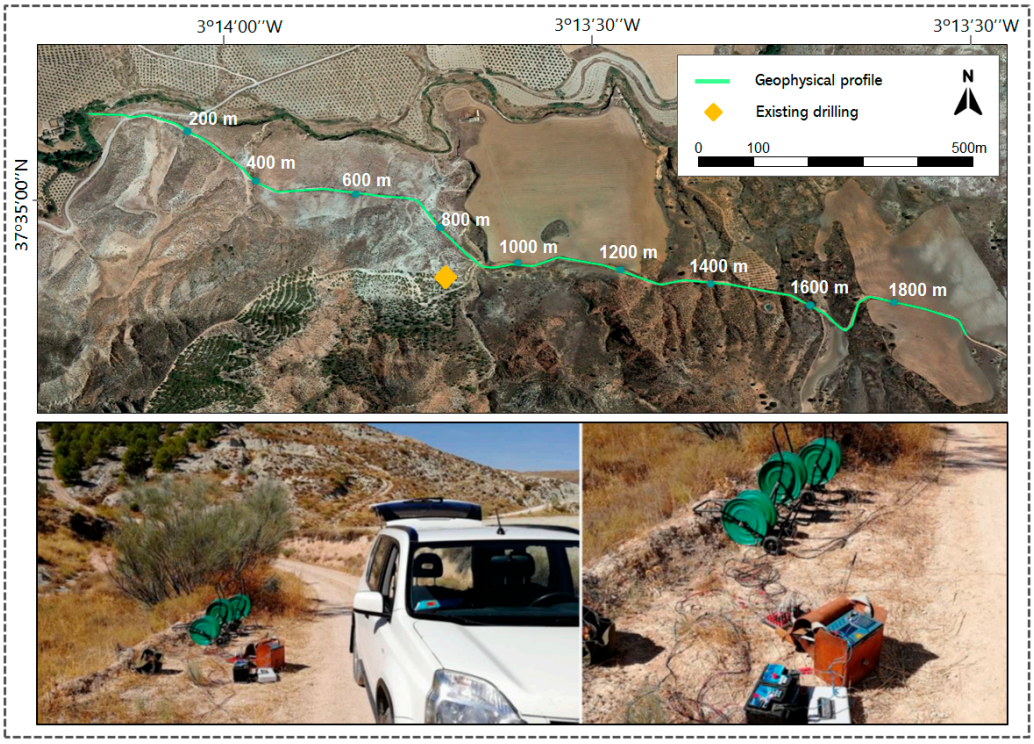

Figure 3. Arrangement of the ERT profile in the area under study (at the **top**) execution of works in the field (at the **bottom**).

Table 2. Description of the lithological column of the existing borehole located in the study area.

Length	Geological Description
0–170 m	Alternations of light and white colors marls assigned to the middle–lower Cretaceous
170–198 m	Alternation of sandy and marl sections with limestone From the Lower Cretaceous and Upper Jurassic
198–214 m	Marls and white limestones from the Middle Jurassic
214–219 m	Tabled limestone and karstified gray dolomitic limestone

3. Materials and Methods

3.1. Geophysical Surveys-ERT

3.1.1. ERT for Geothermal Characterization Review

Based on the description of the previous Sections 2.1 and 2.2, this research aims to determine the in-depth characterization of the structure and arrangement of the subsoil materials and analyze the lateral continuity of the formation of interest, with special attention to the potential presence of fractures. With these objectives in mind, the geophysical-prospecting campaign has been raised considering the partial knowledge of the ground in the study area and the need to reach sufficient depth levels for the investigation here pursued. From the commented initial statements and, as previously mentioned, the electrical-resistivity tomography technique, it was considered as the potential method for the underground evaluation of this work.

ERT survey is widely implemented for mapping the location of potential areas for groundwater, minerals, or geothermal use [27,28]. In the specific geothermal field, different studies have focused on the delineation of geothermal reservoirs and/or associated structures such as fractures or faults as a preliminary prerequisite for a successful geothermal exploration [29]. In the evaluation of large and known geothermal areas, ERT profiles have proven to be a suitable method for obtaining a high spatial variability, where the potential

zone is clearly distinguishable from those with different resistivity [30–32]. In the case of high- and medium-enthalpy geothermal systems, these present great variations in their resistivity/conductivity structure, usually associated with the occurrence of fluids but also with the presence of anomalous concentrations of hydrothermal minerals. The existence of particular fluids, such as saline fluids or meteoric water in rocks, results in enhanced electrical conductivity to a greater or lesser extent, depending on the characteristics of this fluid [33–35]. In these cases, ERT methods are an important source of information, but they also constitute a great help in those surveys where the initial thermal evidence is not so clear, but a possible state of fracturing or structural disposition could indicate the potentiality of geothermal exploitation at different scales. In the case of low- and very-low-enthalpy geothermal resources, these geophysical tools are also extremely valuable for the characterization and distribution of the ground materials and the subsequent design of the well field [18,19].

3.1.2. Fundamentals of the Method and Application on the Study Case

ETR technique provides a subsurface geoelectrical characterization by the measurement of the apparent resistivity from a tetra-electrode device, injecting current of a known intensity into two electrodes called "A" and "B" and automatically recording the potential difference between the other two electrodes "M" and "N". The process is consequently repeated by automatically varying the distances between the pairs of electrodes so that the apparent resistivity is obtained in multiple positions and levels (n). Data are subsequently processed by means of mathematical inversion algorithms, obtaining an image of resistivities and real depths of the subsoil. The depth of investigation is in fact a function of the ability of the material to identify and measure the electric potential between electrodes [36].

The methodology is based on the contrast of resistivities obtained that allows for the differentiation of the subsoil materials based on their electrical behavior; that is, their apparent resistivity value (after the inversion of the field data). However, the subsurface resistivity of a particular area can be affected by different factors such as the porosity and pore structure of the rock formations, the content of water or steam, salinity, pressure, temperature, or any other alteration between water–rock. In this sense, the pore volume, regarding the total rock volume ratio, the geometric arrangement of the pores (formation factor), the ratio of water-filled pores to empty pores, or the resistivity/conductivity of the fluid that is filling the pores [37], is particularly influential.

In the case of the present research, field works consisted of the execution of an electrical tomography profile of 2000 m in length using a hose with 21 electrodes with a separation of 100 m, and a direct and inverse pole–dipole recording device (Figure 3). Data were collected using the commercial equipment Syscal Pro multi-electrode imaging system with an automatic injection range with a 1200 W AC/DC converter. The array configuration was set with the aim of obtaining a strong signal, high-penetration capability, and high-density data. Since the data quality during the ERT acquisition depends on factors such as the noise or the resistivity of materials, the use of a high-power transmitter and an AC/CD converter increases the effective working voltage and contributes to their mitigation. One more influential factor is contact resistance, which is a function of the resistivity of the most superficial layer of the ground. If contact resistances are not allowed, longer and/or multiple linked electrodes are used at the electrode position, and if required, the galvanic contact of electrodes with the ground can be improved by adding a saltwater solution [38]. It is also convenient to mention that the location of each electrode was defined by using a handheld Global Positioning System (GPS) with a horizontal accuracy of 3 m. For the GPS coordinates, ellipsoidal altitudes were also determined since elevation values are required for the subsequent data inversion.

3.1.3. Inversion-Model Approach

Once the ERT raw data on the field (binary) were acquired, these were converted into ASCII format to numerically process the field datasets. For removing the outlier data points,

X2IPI software (version 5.19) was used following the criteria of unmeasured intensities of those values lower than 100 mA [39]. In the next step, topography information was assigned to each node, and the apparent resistivity data were inverted using a linearized least-squares algorithm in order to obtain the inverted resistivity models [40].

Finally, RES2DINV software (version 5.0) was implemented for ERT data modeling. The tool is based on a finite element modeling or a difference algorithm capable of providing the forward modeling of the voltage response to the current injection. The models of resistivity developed by the software are then divided into different rectangular blocks with specific resistivity values coming from the field-measuring process. Data of apparent resistivity are finally presented as a pseudo-section, in which the apparent resistivity values are assigned to a predefined location in function of the type of array [41].

The selected inversion procedure was the smoothness-constrained least-squares optimization method, or the smooth L2 norm (function of a damping factor), which allows for the minimization of the sum of squares between the calculated apparent resistivity values and those observed, producing smooth fluctuations in resistivity within the inversion model. The process of inversion begins with the initial model parameters and the damping factors that are refined through an iterative process.

4. Results

4.1. 2D ERT Profile

Figure 4 shows the results obtained in the 2D ERT profile performed in the area under study. The geoelectrical model also includes the synthetic column crossed by the existing drilling together with the distinction of three main geological horizons and the location of the fault's structures in line with the geological characterization established in Section 2.

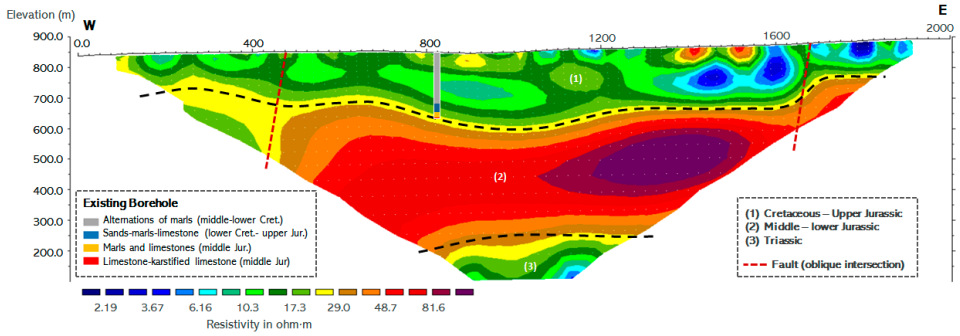

Figure 4. Electrical-resistivity tomography 2D profile in the study area. Length: 2000 m, Interelectrode span: 100 m, Number of electrodes: 21, Dispositive registration: Pole–Dipole, RMS error: 10.3%.

In the 2D model of the above Figure 4, three layers can be distinguished with the following characteristics:

- A first outcropping surface layer (1) of a relatively conductive nature, corresponding to Cretaceous and Upper Jurassic materials mainly constituted by alternations of sandy, limestone, and marly materials. As observed in the 2D profile, Layer (1) presents a more conductive character in the extreme east, indicating the majority presence of clays and marls. Regarding the thickness of the layer, it ranges between 120–250 m.
- An intermediate resistive layer (2), constituted by carbonate materials from the middle and lower Jurassic. This layer has a significant thickness higher than 300 m and presents two main fracture areas (also included in Figure 4):
    - A fracture located around Meter 450 of the 2D profile. The area is defined by the lateral change in resistivity observed in the model that descends at that point in a westerly direction. It should be noted that this fracture context agrees with the fault mapped by the consulted geological database [23], which intersects the trace of the profile at this point, but with a very oblique character.

This factor could influence the resistivity values obtained from the geophysical prospecting campaign.

- A fracture formation appearing approximately at Meter 1700 of the ERT profile, defined by the jump and elevation observed at the top of layer (2), estimated at about 80 m.

- A final conductive basal layer (3), determined by the clear decrease in resistivity, which could indicate the presence of Triassic materials.

In general, the described results indicate that there is an appropriate correlation between the data derived from the existing borehole and the geoelectrical model obtained from geophysics.

4.2. Pseudo-3D ERT Model

In addition to the previous 2D profile, a three-dimensional model has been obtained using Oasis Montaj software (Seequent). Once the profile into the tool is exported, it performs an interpolation of the areas without data from the tomography profile, located in the basal part of the ends. The final product is a 3D geoelectrical model that enables an in-depth analysis of the whole ground distribution [42]. These 3D models are included in the following Figures 5–7 in which it is possible to observe the general structure of the study area in relation to its topography and geological cartography.

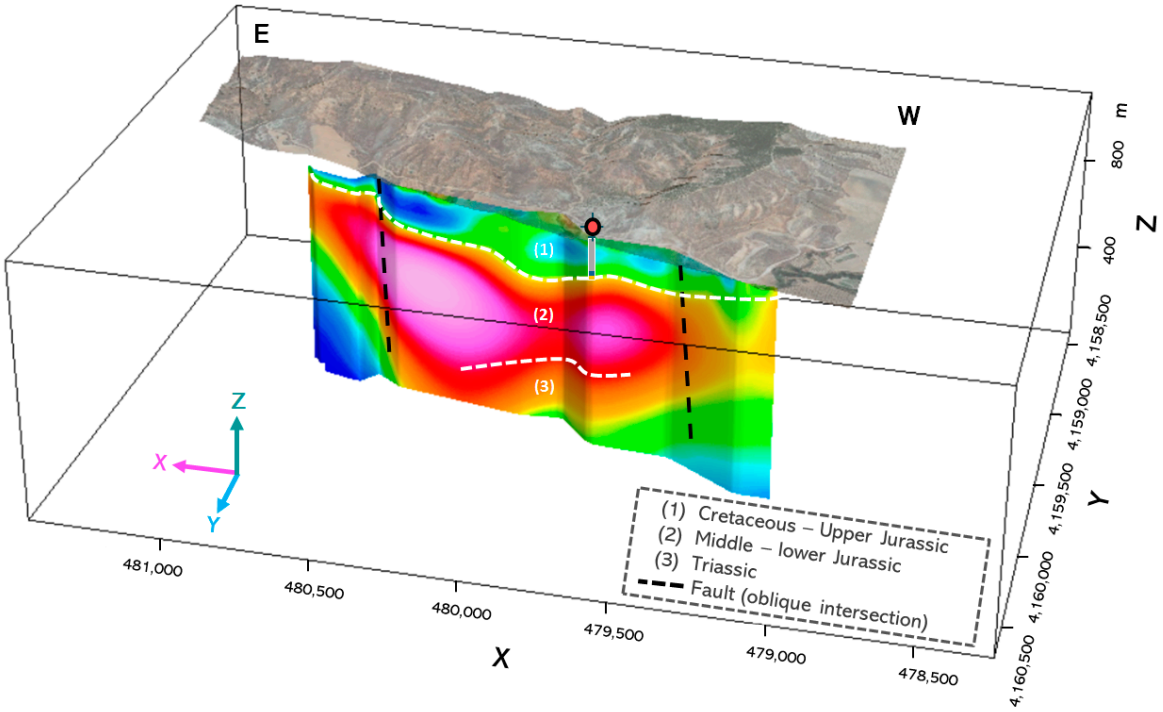

Figure 5. Pseudo 3D model with the digital Terrain Model (DTM) and the orthophoto. View from the north.

The previous Figures 5–7 show the tomography profile obtained from the geophysical campaign (depth information) overlaid with three surface visualization modes: according to the digital model of the terrain and the orthophoto, the single digital terrain model and the digital terrain model together with the geology and family of faults in the area. In all of them, the location of the existing borehole has also been included in order to facilitate the interpretation of the results.

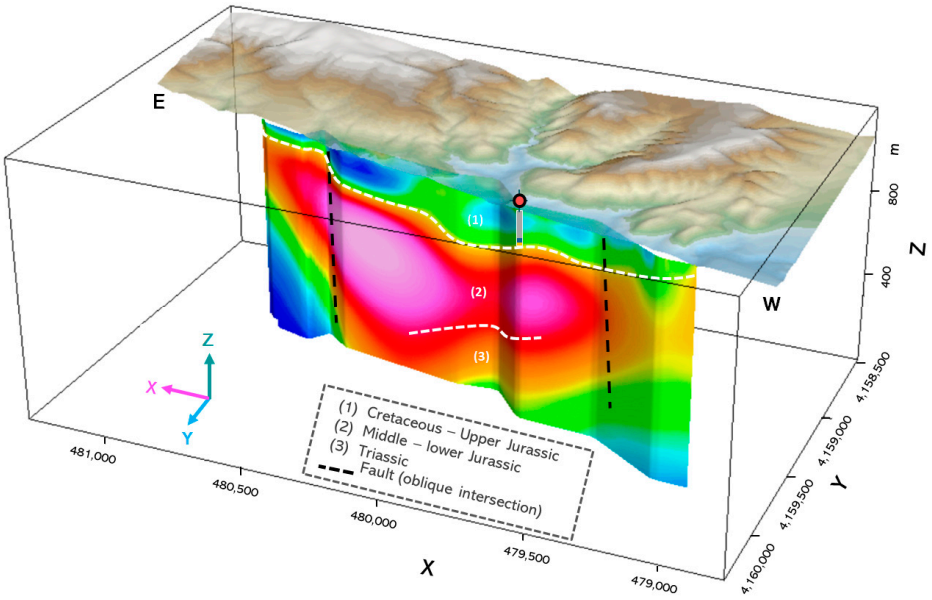

Figure 6. Pseudo-3D model with the Digital Terrain Model (DTM). View from the north.

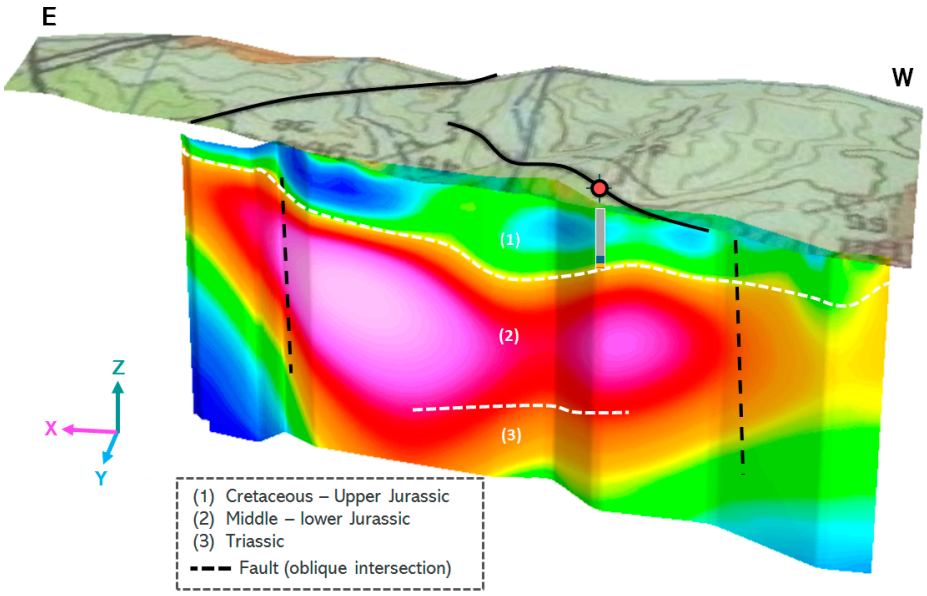

Figure 7. Pseudo-3D model with DTM and geology, highlighting the main mapped faults. View from the north.

5. Discussion

5.1. Model Validation

In certain exploration areas, there is great variability between the geological conditions and the underground distribution. In this sense, the application of geophysics is fundamental for understanding the existing structures and formations in depth. The present research investigates the potential of ERT for the exploration of low–medium enthalpy geothermal resources.

The implementation of an ERT 2000 m long profile has allowed for the penetration of the subsoil up to levels of around 800 m, meaning it is an important source of information about the composition of the materials that make up the subsoil and its distribution in the horizons. The obtained geoelectrical model must represent the subsurface and, at the same time, provide a good fit to the surface geology and lithostratigraphic units based on the existing geological cartography and the known fracture formations and faults.

According to the 1:50,000 scale cartographic layer produced by the IGME (Instituto Geologico y Minero de España) in the area under study, two families of fractures intersect the profile at the eastern and western ends of it. This source of information provides an initial basis for the nature of the characteristic geological formations of the site, which, together with the lithological column known from the borehole existing in the area, represents an important approximation to the characterization of the subsoil. The interpretation of the ERT results agrees with the existing information in the first levels of the ground, also providing additional documentation of how the geological structures are distributed in depth. Through the geophysical campaign, it has been possible to corroborate the arrangement of the fault formations at deeper levels and to characterize the subsoil at greater levels of depth. The results of the survey denote the existence of a potential formation constituted by carbonate materials from the middle and lower Jurassic with a thickness greater than 300 m, which is also crossed by the families of fractures. The set of information provided by the tests and verified by the known structures at more superficial levels makes it possible to accurately plan the most optimal location for possible geothermal exploitation in the analyzed area. The data known from the drilling report of the borehole in the area also confirm (although in much less detail) a significant coincidence in the division of layers in depth.

5.2. Geothermal Exploitation

As commented before, based on the results obtained in the geophysical model, it is possible to establish a preliminary approximation of the most appropriate scenario for future geothermal exploitation. The approach followed here is to evaluate a possible opportunity to semi-directly capture the geothermal flow that is suspected to exist in the underground study area. Due to the limitations of the geophysical techniques (which can only be solved with direct drilling), there is not total certainty about the behavior of the phenomenon, but this section tries to provide a possible exploitation pattern according to the known in-depth information.

Following the geological distribution in the ground, the geothermal drilling should reach the formation (2) of Figures 4–7 in which carbonate materials are present. These layers, characterized in their most superficial part by a certain degree of karstification, constitute a proper environment for the extraction of the required water flow by means of geothermal use. Specifically, the projected borehole should be located at the extreme west of the profile (Figure 8) in the vicinity of the fault structure, and where the formation of interest (2) does not present resistivity values as high as in the case of the existing borehole.

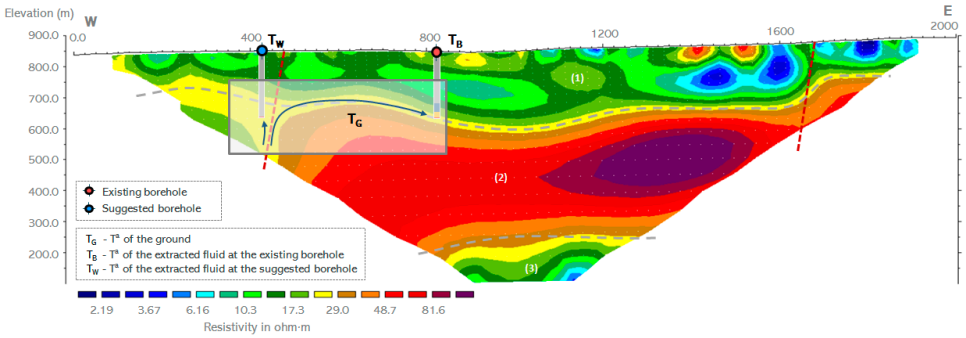

Figure 8. Location of the proposed drilling for possible geothermal exploitation.

Once the potential location for a possible geothermal use is established, an estimation of the temperature of the fluid in the considered area and the possible thermal extraction is presented in this subsection. For this, the probable flow path from the potential area (in the fault) to the existing drilling will be evaluated. Taking into account the geological distribution analyzed in this study, the probable circulation layer should be the one marked in yellow (Figure 8) that communicates the fracture with the lower end of the existing bore-

hole. In this way, and based on the scale of Figure 8, the circulation area is approximately 400 m long and 40 m thick. From this information, and considering the porosity of the limestone formation of the reservoir, the real diameter through which the flow circulates up to the borehole is obtained (D_F of Table 3).

As a second step, it is necessary to define the initial thermal conditions of the site, such as the average temperature of the ground at the depth considered (220 m as the existing drilling). Based on previous studies, the area is not characterized by known significant geothermal anomalies, having a normal geothermal gradient of around 3 °C/100 m and with temperatures within the average values in the original geological environment [43]. The estimated ground temperature at the considered level can be also found in Table 3 as T_G.

Table 3. Principal site and fluid parameters required for the thermal characterization of the site [44].

Main Site Parameters	
Flow diameter (D_F)	3.2 m
Ground Temperature (T_G)	19.5 °C
Temperature of the water borehole (T_B)	35.2 °C
Length of the area (L_A)	400 m
Thickness of the area (T_A)	40 m
Considered depth (D_P)	220 m
Fluid Properties	
Kinematic viscosity (υ)	1×10^{-6} m^2/s
Dynamic viscosity (μ)	1×10^{-3} kg/m·s
Specific heat (c_p)	4184 J/kg·K
Thermal conductivity (k)	0.6 W/m·K

Based on the above information, the heat flux by forced convection can be evaluated, for which different parameters must be defined. The first one is the dimensionless Reynolds number (Re), required to categorize the fluid of the system and to confirm the laminar behavior of the flow (Equation (1)) [45].

$$Re = \frac{V \cdot D_F}{\upsilon} \quad (1)$$

where V is the average flow velocity (m/s).

In the present study case, the flow velocity (V) is estimated according to measurements obtained from the existing borehole, such as the transmissivity of 600 m^2/day already mentioned in Section 2.2 and the analyzed layer thickness (T_A), obtaining a maximum flow velocity of around 15 m/day. Regarding the kinematic viscosity (υ), it is consulted in standard databases for water at the temperature of the medium considered (Table 3) [43]. With all these values, a Reynolds number of 555.56 is obtained, denoting the laminar nature of the fluid in the analysed conditions of the environment.

The following parameters to calculate are the Prandtl number (Pr), which expresses a dimensionless quantity for assessing the relation between momentum transport and thermal transport capacity of the fluid, and the Nusselt number (Nu) that is basically a function of Re and Pr numbers. Both numbers are defined in Equations (2) and (3) [45].

$$Pr = \frac{\mu \cdot C_p}{k} \quad (2)$$

$$Nu = 3.66 + \frac{0.065 \cdot \left(\frac{D_F}{L_A}\right) \cdot Re \cdot Pr}{1 + 0.04 \cdot \left[\left(\frac{D_F}{L_A}\right) \cdot Re \cdot Pr\right]^{2/3}} \quad (3)$$

Considering again the standard values of μ, $c_{p,}$ and k for the fluid at the analyzed conditions (Table 3) [46], Pr and the Nu numbers are estimated as 6.97 and 5.26, respectively. It is convenient to mention that Equation (3) provides an approximation to the calculation of Nu, considering that the value obtained is greater than 3.66 as the one here presented.

Once defined, the previous parameters, the thermal convection coefficient (h) (W/m^2·K) for forced convection, is expressed as follows (Equation (4)).

$$h = \frac{k}{D_F} \cdot Nu \quad (4)$$

Substituting the corresponding values, the convection coefficient h for the study conditions is 0.99 W/m^2·K. Convective heat transfer occurs from the moving of the fluid through the considered formation, according to what is known as Newton's Law of Cooling. In this way, from the calculated convection coefficient, the temperature of the water (T_W) in the suggested location of the fracture can be calculated by applying Equation (5) [47].

$$T_W = T_{G-} \left[\frac{T_G - T_B}{e^{-\frac{h \cdot A_s}{\dot{m} \cdot c_p}}} \right] \quad (5)$$

where A_s (m^2) is the area through which the fluid circulates in the formation and $\dot{m}$ (kg/s) is the mass flow rate.

Considering the geometry of the formation, as well as the density and the estimated velocity of the fluid, A_s and $\dot{m}$ can be directly obtained, being the values 3516.80 m^2 and 1.40 kg/s, respectively. Finally, applying the previous Equation (5), the water temperature in the area suggested in this study could reach the value of 48.89 °C.

On top of the above, the specific energy (E) that the increase in temperature supposes in both conditions (in the existing drilling and in the suggested one) is calculated applying the following equation.

$$E = c_p \cdot \Delta T \cdot m \quad (6)$$

where m (kg/h) is the mass of the circulating fluid, which can be calculated from the estimated flow in the existing drilling (at least 60 L/s) that, considering the density of the fluid, is means 216,000 kg/h. ΔT (°C) is the temperature increase between the ground and the temperature of the water in each assumption. These values, and the final result of applying Equation (6), are included in Table 4.

Table 4. Increase in temperature and specific energy achieved in each of the considered scenarios.

Scenario	Δ*T* (°C)	*E* (*J*)	*E* (*th*)
Existing drilling	15.70	1.42×10^{10}	3388.93
Suggested drilling	29.39	2.66×10^{10}	6343.99

From the previous values of Table 4, it is easily observable how the extraction of water in the area suggested in the present research supposes an increase in temperature of almost double that currently achieved in the existing borehole of the area. All this also means doubling the specific energy of the site and denoting the presence of a relevant geothermal resource of significant importance for its future use.

In relation to the previous calculations of the upwelling temperature, it should be clarified that this is one of the possible scenarios regarding the origin of the thermal anomaly measured in the well. For a deeper characterization of the resource, it would be necessary to take into account possible deviations in the geometry and properties of the geological

structure that constitute the aquifer (error of the inversion process of geophysical data), or possible thermal contributions not considered in the direction of the flow prior to the emerging fracture.

6. Conclusions

In different regions of Spain, the lack of precise information on the resource and its possibilities of exploitation constitute a barrier preventing geothermal energy from making a greater contribution to meeting energy demand at present. The present study applies deep electrical-resistivity tomography to characterize a possible geothermal site. The information about the subsoil obtained from the resistivity data is in agreement with the geological structures known from the existing borehole located in the vicinity of the studied area. Beyond this contribution, the geophysical campaign has allowed to know the distribution of the geological formations and structures at greater depth and define the ideal location for better geothermal resource exploitation. In this way, and by locating the possible energy source in depth through the structuring in the form of a fault, the extraction of water in the proposed area allows us to achieve an estimated temperature of 48 °C with an energy use of practically double the current extraction in the existing borehole.

Based on all that has been evaluated in this investigation, future geothermal exploitation initiatives in the study area will be precisely planned, minimizing the possibilities of error and facilitating the corresponding exploration and implementation tasks linked to the geothermal-extraction system. Regarding future research, and since it is a promising area, it would be interesting to address the analysis of the formations that give rise to thermal anomalies on the surface through the use of more extensive geophysical techniques. In this sense, the application of the magnetotelluric method could be advisable to image the subsurface electrical resistivity and provide (by the use of the Earth's naturally occurring electromagnetic fields) useful information about the lateral and vertical resistivity variation. The investigation depth of this technique can reach several tens of kilometers in function on rock resistivity, making it a technology of great value to be applied in areas such as the one evaluated in this research, making it also possible to determine with greater precision the scope of the resource and its possibilities of use as a medium or a high-enthalpy geothermal system.

Author Contributions: Conceptualization, C.S.B. and I.M.N.; methodology, C.S.B.; software, P.C. and J.C.; validation, A.F.M. and D.G.-A.; formal analysis, C.S.B., I.M.N. and M.Á.M.-G.; investigation, C.S.B.; resources, P.C., D.P. and J.C.; data curation, P.C., D.P. and J.C.; writing—original draft preparation, C.S.B.; writing—review and editing, C.S.B.; visualization, M.Á.M.-G.; supervision, A.F.M. and D.G.-A.; project administration, C.S.B.; funding acquisition, A.F.M., C.S.B. and M.Á.M.-G. All authors have read and agreed to the published version of the manuscript.

Funding: This research was supported by the research projects support program and cofinanced by the European Regional Development Fund (ERDF) under the order of the Ministry of Education from Castilla y León (project ref.: SA102P20). "Development and integration of a new district heating system using low-energy geothermal energy (GEO-DISTRICT 3.0)" and the European Union's Horizon 2020 research and innovation programme under grant agreement nº 101091885 (Mine.io project). M.Á.M.-G. and C.S.B. acknowledge the grant RYC2021-034813-I and RYC2021-034720-I, respectively, funded by MCIN/AEI/10.13039/501100011033 and by European Union "NextGenerationEU"/PRTR.

Data Availability Statement: Data will be available when required.

Acknowledgments: Authors would also like to thank the Department of Cartographic and Land Engineering of the Higher Polytechnic School of Avila, University of Salamanca for allowing us to use their facilities and their collaboration during the experimental phase of this research.

Conflicts of Interest: The authors declare no conflicts of interest.

Nomenclature

Acronyms

GHP	Geothermal Heat Pump
GSHP	Ground-Source Heat Pump
GWHP	Ground-Water Heat Pump
NZEB	Nearly Zero-Energy Building
ERT	Electrical-Resistivity Tomography
GPS	Global Positioning System
IGME	Instituto Geológico y Minero de España
D_F	Flow diameter
T_G	Ground Temperature
T_B	Temperature of the water borehole
T_W	Temperature of the water
L_A	Length of the area
T_A	Thickness of the area
D_P	Considered depth
υ	Kinematic viscosity
v	Flow velocity
μ	Dynamic viscosity
c_p	Specific heat
k	Thermal conductivity
Re	Reynolds number
Pr	Prandtl number
Nu	Nusselt number
h	Thermal convection coefficient
A_s	Area of circulation of the fluid in the formation
$\dot{m}$	Mass flow rate
E	Specific energy
m	Mass of the circulating fluid

References

1. Fridleifsson, I.B. Geothermal energy for the benefit of the people. *Renew. Sustain. Energy Rev.* **2001**, *5*, 299–312. [CrossRef]
2. García-Gil, A.; Goetzl, G.; Kłonowski, M.R.; Borovic, S.; Boon, D.P.; Abesser, C.; Janza, M.; Herms, I.; Petitclerc, E.; Erlström, M.; et al. Governance of shallow geothermal energy resources. *Energy Policy* **2020**, *138*, 111283. [CrossRef]
3. Dickson, M.H.; Fanelli, M. *Geothermal Energy: Utilization and Technology*; Routledge: London, UK, 2013; ISBN 978-1-84407-184-5.
4. Lund, J.W.; Toth, A.N. Direct utilization of geothermal energy 2020 worldwide review. *Geothermics* **2021**, *90*, 101915. [CrossRef]
5. Sáez Blázquez, C.; Martín Nieto, I.; Farfán Martín, A.; González-Aguilera, D.; Carrasco García, P. Comparative analysis of different methodologies used to estimate the ground thermal conductivity in low enthalpy geothermal systems. *Energies* **2019**, *12*, 1672. [CrossRef]
6. Limberger, J.; Boxem, T.; Pluymaekers, M.; Bruhn, D.; Manzella, A.; Calcagno, P.; Beekman, F.; Cloetingh, S.; van Wees, J.-D. Geothermal energy in deep aquifers: A global assessment of the resource base for direct heat utilization. *Renew. Sustain. Energy Rev.* **2018**, *82*, 961–975. [CrossRef]
7. Rybach, L. Global Status, Development and Prospects of Shallow and Deep Geothermal Energy. *Int. J. Terr. Heat Flow Appl. Geotherm.* **2022**, *5*, 20–25. [CrossRef]
8. Lund, J.W.; Huttrer, G.W.; Toth, A.N. Characteristics and trends in geothermal development and use, 1995 to 2020. *Geothermics* **2022**, *105*, 102522. [CrossRef]
9. Blázquez, C.S.; Borge-Diez, D.; Nieto, I.M.; Martín, A.F.; González-Aguilera, D. Multi-parametric evaluation of electrical, biogas and natural gas geothermal source heat pumps. *Renew. Energy* **2021**, *163*, 1682–1691. [CrossRef]
10. D'Agostino, D.; Mazzarella, L. What is a Nearly zero energy building? Overview, implementation and comparison of definitions. *J. Build. Eng.* **2019**, *21*, 200–212. [CrossRef]
11. Blázquez, C.S.; Borge-Diez, D.; Nieto, I.M.; Martín, A.F.; González-Aguilera, D. Technical optimization of the energy supply in geothermal heat pumps. *Geothermics* **2019**, *81*, 133–142. [CrossRef]
12. Magrini, A.; Lentini, G.; Cuman, S.; Bodrato, A.; Marenco, L. From nearly zero energy buildings (NZEB) to positive energy buildings (PEB): The next challenge-The most recent European trends with some notes on the energy analysis of a forerunner PEB example. *Dev. Built Environ.* **2020**, *3*, 100019. [CrossRef]
13. Sorman, A.H.; García-Muros, X.; Pizarro-Irizar, C.; González-Eguino, M. Lost (and found) in Transition: Expert stakeholder insights on low-carbon energy transitions in Spain. *Energy Res. Soc. Sci.* **2020**, *64*, 101414. [CrossRef]

14. Arrizabalaga, I.; De Gregorio, M.; De Santiago, C.; García de la Noceda, C.; Pérez, P.; Urchueguía, J.F. Country update for the Spanish geothermal sector. In Proceedings of the World Geothermal Congress, Melbourne, Australia, 19–24 April 2015; pp. 19–24.
15. Arrizabalaga, I.; De Gregorio, M.; De Santiago, C.; García de la Noceda, C.; Pérez, P.; Urchueguía, J.F. Country update for the Spanish geothermal sector. In Proceedings of the World Geothermal Congress, Reykjavik, Iceland, 27 April–1 May 2020; p. 12.
16. Vivas, C.; Salehi, S.; Tuttle, J.D.; Rickard, B. Challenges and opportunities of geothermal drilling for renewable energy generation. *GRC Trans.* **2020**, *44*, 904–918.
17. Anderson, A.; Rezaie, B. Geothermal technology: Trends and potential role in a sustainable future. *Appl. Energy* **2019**, *248*, 18–34. [CrossRef]
18. Blázquez, C.S.; Nieto, I.M.; González, M.Á.M.; García, P.C.; Martín, A.F.; González-Aguilera, D. Geophysical exploration for shallow geothermal applications: A case study in Artà, (Balearic Islands, Spain). *Geothermics* **2022**, *105*, 102517. [CrossRef]
19. Sáez Blázquez, C.; Carrasco García, P.; Nieto, I.M.; Maté-González, M.Á.; Martín, A.F.; González-Aguilera, D. Characterizing geological heterogeneities for geothermal purposes through combined geophysical prospecting methods. *Remote Sens.* **2020**, *12*, 1948. [CrossRef]
20. Carrier, A.; Fischanger, F.; Gance, J.; Cocchiararo, G.; Morelli, G.; Lupi, M. Deep electrical resistivity tomography for the prospection of low-to medium-enthalpy geothermal resources. *Geophys. J. Int.* **2019**, *219*, 2056–2072. [CrossRef]
21. Nieto, I.M.; Carrasco García, P.; Sáez Blázquez, C.; Farfán Martín, A.; González-Aguilera, D.; Carrasco García, J. Geophysical prospecting for geothermal resources in the south of the Duero Basin (Spain). *Energies* **2020**, *13*, 5397. [CrossRef]
22. Ismail, N.; Syukri, M.; Idroes, R. Deep and shallow structures of geothermal Seulawah Agam based on electromagnetic and magnetic data. *Geomate J.* **2019**, *16*, 141–147. [CrossRef]
23. Mohamed, M.A.; Pajares, A.J.M.; Moreno, J.L.; Herrador, M.B.; Álvarez, F.P.; Reyes, J.M.G. Phylogenetic relationships of "Erysimum"(Brassicaceae) from the Baetic Mountains (SE Iberian Peninsula). In *Anales del Jardín Botánico de Madrid*; Real Jardín Botánico: Madrid, Spain, 2014; Volume 71, p. 5. [CrossRef]
24. Sala, M. Baetic Cordillera and Guadalquivir Basin. In *Geomorphology of Europe*; Palgrave: London, UK, 1984; pp. 323–340. [CrossRef]
25. Albir, A.E.; López Olmedo, F.L.; Díaz de Neira, J.A. Mapa y memoria explicativa de la Hoja 970, El Rubio. MAGNA. IGME. 1981.
26. Guzmán, S.J. *Sondeo de Agua Minero Industrial de Origen Termal "Alamedilla 1" Capacity Report*; Junta de Andalucía: Andalusia, Spain, 2015.
27. Lévy, L.; Maurya, P.K.; Byrdina, S.; Vandemeulebrouck, J.; Sigmundsson, F.; Árnason, K.; Ricci, T.; Deldicque, D.; Roger, M.; Gibert, B.; et al. Electrical resistivity tomography and time-domain induced polarization field investigations of geothermal areas at Krafla, Iceland: Comparison to borehole and laboratory frequency-domain electrical observations. *Geophys. J. Int.* **2019**, *218*, 1469–1489. [CrossRef]
28. Singh, S.; Gautam, P.K.; Bagchi, D.; Singh, S.; Kumar, S.; Kannaujiya, S. 2D electrical resistivity imaging for geothermal groundwater characterization and rejuvenation of the Gaurikund hot spring in the Main Central Thrust (MCT) zone of the Garhwal Himalaya, Uttrakhand, India. *Groundw. Sustain. Dev.* **2021**, *15*, 100686. [CrossRef]
29. Kumar, D.; Thiagarajan, S.; Rai, S.N. Deciphering geothermal resources in Deccan Trap region using electrical resistivity tomography technique. *J. Geol. Soc. India* **2011**, *78*, 541–548. [CrossRef]
30. Vanhooren, L.; Fontaine, O.; Caudron, C.; Vrancken, E.; Dekoninck, W.; De Lathauwer, H.; Hermans, T. *Characterization and Monitoring of the Gunnuhver Geothermal Site Using Electrical Methods (No. EGU23-12873)*; Copernicus Meetings; EGU: Vienna, Austria, 2023. [CrossRef]
31. Cheng, Y.; Wang, C.; Da, W.; Kong, Y.; Hu, X. Anatomy of the convective geothermal system from geophysical and hydrochemical data: A case study from the Changshou geothermal field, South China. *Geophysics* **2023**, *88*, 1–43. [CrossRef]
32. Ussher, G.; Harvey, C.; Johnstone, R.; Anderson, E. Understanding the resistivities observed in geothermal systems. In Proceedings of the World Geothermal Congress, Kyushu, Japan, 28 May–10 June 2000; pp. 1915–1920.
33. Marwan, M.; Isa, M.; Idroes, R.; Nursyafira, N.; Idris, S.; Yanis, M.; Ghani, A.A.; Paembonan, A.Y. Geoelectrical Model of Geothermal Spring in ie Jue Seulawah Deriving from 2D Vlf-Em and dc Resistivity Methods. *J. Appl. Eng. Sci.* **2023**, *21*, 59–69. [CrossRef]
34. Abdullah, A.I.; Musa, M.D.T.; Uno, I.; Jayadi, H. Resistivity model of hallow subsurface to find the path of geothermal manifestation in Bora Village of Sigi Regency of Central Sulawesi. *J. Phys. Conf. Ser.* **2019**, *1242*, 012048. [CrossRef]
35. Cumming, W.; Mackie, R. Resistivity imaging of geothermal resources using 1D, 2D and 3D MT inversion and TDEM static shift correction illustrated by a Glass Mountain case history. In Proceedings of the World Geothermal Congress, Bali, Indonasia, 25–30 April 2010; pp. 25–29.
36. Arjwech, R.; Everett, M.E. Application of 2D electrical resistivity tomography to engineering projects: Three case studies. *Songklanakarin J. Sci. Technol.* **2015**, *37*, 675–681.
37. Zhou, B.; Bouzidi, Y.; Ullah, S.; Asim, M. A full-range gradient survey for 2D electrical resistivity tomography. *Near Surf. Geophys.* **2020**, *18*, 609–626. [CrossRef]
38. Carrasco García, P. Avance en Técnicas Geofísicas Para la Caracterización del Subsuelo Mediante Innovación y el Uso de Herramientas de Gestión de Información Espacial. Ph.D. Thesis, Escuela Politécnica Superior de Ávila, Univ de Salamanca, Ávila, Spain, 2013; p. 523.
39. Robain, H.; Bobachev, A. X2IPI Toolbox for 2D DC measurements with SYSCAL equipment. *User manual*, 2002; 25p.

40. Loke, M.H.; Dahlin, T. A comparison of the Gauss–Newton and quasi-Newton methods in resistivity imaging inversion. *J. Appl. Geophys.* **2002**, *49*, 149–162. [CrossRef]
41. Telford, W.M.; Telford, W.M.; Geldart, L.P.; Sheriff, R.E. *Applied Geophysics*; Cambridge University Press: Cambridge, UK, 1990; ISBN 1139642928/9781139642927.
42. Arifin, M.H.; Kayode, J.S.; Ismail, K.I.; Abdullah, M.; Embrandiri, A.; Nazer, S.M.; Azmi, A. Data for the industrial and municipal environmental wastes hazard contaminants assessment with integration of RES2D techniques and Oasis Montaj software. *Data Brief* **2020**, *33*, 106595. [CrossRef]
43. Galindo-Zaldívar, J.; Jabaloy, A.; Serrano, I.; Morales, J.; González-Lodeiro, F.; Torcal, F. Recent and present-day stresses in the Granada Basin (Betic Cordilleras): Example of a late Miocene-present-day extensional basin in a convergent plate boundary. *Tectonics* **1999**, *18*, 686–702. [CrossRef]
44. Mao, Y.; Zhang, Y. Thermal conductivity, shear viscosity and specific heat of rigid water models. *Chem. Phys. Lett.* **2012**, *542*, 37–41. [CrossRef]
45. Abraham, J.P.; Sparrow, E.M.; Tong, J.C.K. Heat transfer in all pipe flow regimes: Laminar, transitional/intermittent, and turbulent. *Int. J. Heat Mass Transf.* **2009**, *52*, 557–563. [CrossRef]
46. Crittenden, J.C.; Trussell, R.R.; Hand, D.W.; Howe, K.J.; Tchobanoglous, G. *MWH's Water Treatment: Principles and Design*, 3rd ed.; John Wiley & Sons: Hoboken, NJ, USA, 1861; ISBN 978-0-470-40593-0.
47. Domenico, P.A.; Palciauskas, V.V. Theoretical analysis of forced convective heat transfer in regional ground-water flow. *Geol. Soc. Am. Bull.* **1973**, *84*, 3803–3814. [CrossRef]